Available online at www.sciencedirect.com

ScienceDirect

Advances in Space Research 67 (2021) 4177–4192

ADVANCES IN SPACE RESEARCH
(a COSPAR publication)

www.elsevier.com/locate/asr

Assessment of the close approach frequency and collision probability for satellites in different configurations of large constellations

Alexis Petit [a,b,*], Alessandro Rossi [a], Elisa Maria Alessi [c]

[a] IFAC-CNR, Via Madonna del Piano 10, 50019 Sesto Fiorentino, FI, Italy
[b] Space Dynamics Services s.r.l., Via Mario Giuntini, 63, 56023 Navacchio di Cascina PI, Italy
[c] IMATI-CNR, via Alfonso Corti 12, 20133 Milano, Italy

Received 5 April 2020; received in revised form 14 January 2021; accepted 14 February 2021
Available online 24 February 2021

Abstract

The Earth orbital environment is drastically changing due to an intensification of the space activities. In particular, several projects of large constellations, proposed for the next years for communications purpose like global internet access, Internet of Things, or for Earth observations, will lead to the deployment of several thousands of new satellites at an unprecedented rate. It is a crucial challenge for space traffic management, which will deal with a great number of satellite conjunctions, potentially causing a collision with damaging consequences for the constellation itself and the space environment sustainability.

In this paper, we investigate the close approach frequency and the cumulative collision probability for each referenced constellation. For this purpose, we compute the orbital evolution of satellites in different constellations during the lifecycle, from the deployment to the decommissioning, and we apply the CUBE algorithm and the Foster method to assess the collision probability with the background space debris population assuming a constant uncertainty in position. We show the variation of risk defined by the close approach frequency and the cumulative collision probability as a function of the proposed configuration. In particular, satellites of the Iridium and Kuiper constellation, but also satellite of the Telesat constellation on polar orbits are the most exposed at a collision. Moreover, the decommissioning phase contribute for a major part to the final cumulative collision probability.
© 2021 COSPAR. Published by Elsevier B.V. All rights reserved.

Keywords: Space debris; Large satellite constellations; Collision probability

1. Introduction

The population of satellites in the Earth orbital environment is dramatically increasing. In the low Earth orbit (LEO) region (altitudes below 2000 km) several space companies are deploying large satellite constellations involving several hundreds to several thousands satellites.

In absence of an effective space traffic management system, the manoeuvres in space are often not well known in advance by whole the space community, the operators communicate partially about the real state of the satellites, and no rule exists in order to organize problematic situation like close approaches.

A satellite of the Starlink constellation has already experienced a conflicting close approach with the ESA's satellite Aeolus on Monday, 2 September, 2019.[1] This is an example of how the space traffic is becoming a hot topic for the space community because of the increasing collision risk in a context of large uncertainty and a lack of knowledge.

* Corresponding author.
E-mail addresses: a.petit@ifac.cnr.it (A. Petit), a.rossi@ifac.cnr.it (A. Rossi), em.alessi@mi.imati.cnr.it (E.M. Alessi).

[1] https://www.esa.int/Our_Activities/Space_Safety/ESA_spacecraft_dodges_large_constellation.

https://doi.org/10.1016/j.asr.2021.02.022
0273-1177/© 2021 COSPAR. Published by Elsevier B.V. All rights reserved.

The assessment of the collision risk, in term of conjunction rate or probability, faced by a given mission is a crucial design parameter, because it gives an estimate of the number of collision avoidance manoeuvres needed during the different phases of the mission, from the deployment to the disposal. For the space operators, a manoeuvre has a cost because it consumes propellant and reduces the operational life. On the other hand, a collision could damage a satellite, and even worst, create new fragments threatening other satellites, and in turn the sustainability of the whole orbital space environment. Investigations about the collision avoidance manoeuvre rate of different space missions will provide information on the level of pressure the future space environment will be subject to.

The mitigation guidelines aim at preserving the space environment and the sustainability of the space activities in the long-term (Inter-Agency Space Debris Coordination Committee, 2007). For example, in LEO it is recommended that the lifetime of a given object is lower than 25 years after its operational life. Moreover, in the context of the large constellations (Lewis et al., 2017), it was shown that the decommissioning success is of paramount importance to control the population growth and post-mission disposal success rates around 90% are required (Virgili et al., 2016). On top of that a very effective and reliable collision avoidance system, with success rate close to 100 %, shall be implemented (Lewis et al., 2017; Virgili et al., 2016). Hence, intensive efforts must be devoted to the collision risk reduction during the different phases of the orbital life of satellites constellations.

Several studies have investigated the interaction between the large constellations and the background environment of satellites and space debris. Based on an estimation of the flux of space debris, they compute the collision rate or the collision probability using Poisson statistics. It was found for all satellites of the OneWeb constellation, during a complete lifecycle, a total collision probability of 35% with objects larger than 3 cm, and of 13.45% during the operational phase at 1200 km of altitude (Radtke et al., 2017). Another study has found a probability of 5% that at least one catastrophic collision occurs during the operational phase of OneWeb (720 satellites located at an altitude of 1200 km) and of 45.8% for Starlink (4425 satellites located between 1110 km and 13255 km of altitude), let almost a difference of a factor of 10 (May et al., 2018). Respectively for OneWeb and Space X, a Business-as-Usual scenario of the background environment leads to 5 and 304 collisions with trackable and non-trackable objects over a period of 5 years.

In the FCC filings, companies like Space X or Kuiper describe their future constellations and they include a brief analysis of the collision probability. In particular, Space X provides a collision probability in case of satellite failure on the injection orbit or on the nominal orbits, in different configurations (stowed or deployed), and until the natural atmospheric reentry[2]. In case of failure on the injection orbit (an elliptical orbit with an apogee of 370 km and a perigee of 210 km), the collision probability varies between $1.44 \cdot 10^{-8}$ to $3.01 \cdot 10^{-8}$. A table gives the collision probability in case of failure at altitudes between 328 km of altitude and 614 km varying between $6.2 \cdot 10^{-8}$ and $2.867 \cdot 10^{-4}$. In the same way, a collision probability of $1.1 \cdot 10^{-7}$ was assessed by Amazon in case of failure at 350 km in the stowed configuration and of $1.265 \cdot 10^{-6}$ in the unstowed configuration. In case of failure on the operational orbit (between 590 and 630) the collision probability varies between $2.084 \cdot 10^{-4}$ and $5.170 \cdot 10^{-4}$. [3] Unfortunately, no information are provided about the frequency of conjunctions and collision avoidance manoeuvres expected.

Moreover, the design of scheduled large constellations is regularly changing, and new projects are coming, making the situation more complex. Thus, we propose a complementary analysis, based on an implementation of the well-known CUBE algorithm used by space debris models, for each of the scheduled large constellations. We are also motivated by the possibility to obtain an accurate description of the close approaches saving the dynamical states of the target and chaser bodies. Filling a database of close approaches for different space missions will help to define the strategies needed in terms of collision avoidance manoeuvres to ensure the safety.

In Section 2, we introduce the main projects of large constellations. In Section 3, we describe our orbit propagator and the manoeuvres followed by a satellite during its full lifecycle. In Section 4, we describe the implementation of the CUBE algorithm to detect conjunctions between a target satellite and the background environment and the Foster method to assess the collision probability. In Section 5, we compute the number of close approaches and the cumulative collision probability of individual satellites of large constellations introduced and for the different phases of the orbital life, from the orbit raising to the decommissioning. Finally, in Section 6 we draw some conclusions.

2. The main projects of large constellations

2.1. Description

During the recent years, some large constellations have been announced. They have different configurations in terms of altitude, number of orbital planes and satellites number. In Table 1, we summarize the characteristics of the main large constellations. Up to November 11, 2019, the largest constellation has been for almost two decades the Iridium constellation (renamed Iridium NEXT after

[2] FCC file #SAT-LOA-20200526–00055, Technical Attachment p.45–46.

[3] https://licensing.fcc.gov/myibfs/download.do?attachment_key=1912531.

Table 1
Characteristics of the satellite constellations Iridium NEXT, OneWeb, Starlink, Telesat, and Kuiper, and Kepler. We note the Starlink and Telesat constellations are split in two parts, and Kuiper in three parts.

Name	Altitude (km)	i (deg)	Orbital planes P	Satellites T
Starlink VLEO	335.9, 340.8, 345.6,	42, 48, 53	1, 1, 1	2547, 2547, 2547
Starlink	550	53	72	1594
Kepler	575	89.5	7	140
Kuiper	590, 610, 630	33, 42, 51.9	28, 36, 34	784, 1296, 1156
Iridium NEXT	780	86.4	6	66
Telesat (polar)	1015	98.98	27	351
OneWeb	1200	87.9	18	720
Telesat (inclined)	1325	50.88	40	1320
Starlink	1110, 1130, 1275, 1325	53.8, 74, 81, 70	32, 8, 5, 6	1600, 400, 375, 450

its replacement) with 66 satellites, and it was surpassed by a factor 10 in satellite number by Starlink in June 2020.

The design of a large constellation is driven by several constraints (leaving aside any consideration about bandwidth and transmission power). A lower altitude leads to a higher number of satellites to maintain a full coverage of the Earth surface. In low altitude, the atmospheric drag must be compensated by frequent orbit raising manoeuvres. On the other hand, a location at a higher altitude leads to cross crowded regions during the deployment and the decommissioning, increasing the complexity of the space traffic management. In general, the location of the constellation is mainly constrained by the region of lowest space object density. In Fig. 1, the density is plotted as a function of the altitude of the resident space objects (RSO) in LEO extracted from the USSTRATCOM catalog at the date of March 1st, 2020. In the same figure, we also show the location of the large constellations. OneWeb, Starlink VLEO, or Telesat are in a region less crowded in order to reduce the close approaches and the number of collision avoidance manoeuvres. Starlink and Kuiper are close to a region of high density. However, they avoid to cross the region of maximum density at 800 km of altitude, and in case of loss of control, the atmospheric drag allows a natural atmospheric reentry in limited number of years (well below the usual 25 years).

We note that the plans of the different operators are regularly changing for some economic and strategic reasons. The values given come from those validated by the Federal Communications Commission (FCC) or announced publicly by the operators.

2.1.1. Iridium NEXT

The deployment of the first generation of Iridium satellites started in 1999 and was entirely replaced by the satellites of second generation named Iridium NEXT, by the use of 8 launches of Falcon 9, with the first launch on January 14, 2017 and the last launch on January 11, 2019.

The constellation contains 66 satellites placed at 781 km of altitude, distributed into six orbital planes inclined at 86.4 degrees, and spaced by 30 degrees. Moreover, the phasing repeats every two planes. Based on the EliteBus™100 platform, each satellite has a mass of 840 kg, a shape of 3.1 m × 2.4 m × 1.5 m, and a wingspan of 9.4 m with the solar panels. It is propelled by 9 monopropellant hydrazine thrusters.

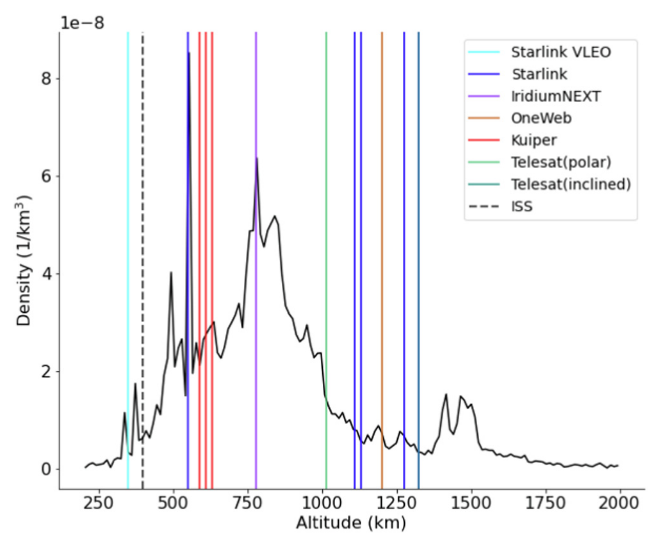

Fig. 1. Density of the objects in the LEO region computed from the TLE catalog of the USSTRATCOM at the date of 1st March 2020 using the data available on the website www.space-track.org. The vertical lines give the location of the large constellations. The dashed line gives the location of the ISS.

The launchers carried up a bunch of 10 satellites which was placed into a circular orbit at 625 km of altitude, and each satellite was released approximately at an interval of 100 s. One by one, they used their own thrusters to reach their nominal altitude of 780 km. In Fig. 2, the semi-major axis of the Iridium satellites are plotted, showing the decommissioning until the atmospheric reentry of the first generation of satellites and the deployment of the new ones. At the end of the planned 15-year lifetime, the satellites are placed on a disposal orbit. First, they are removed from the constellation by lowering the altitude at 750 km. Second, the perigee is lowered to 500 km of altitude. A budget of 39.6 kg of fuel is allocated for these manoeuvres. Then, an atmospheric reentry occurs in less than 25 years.

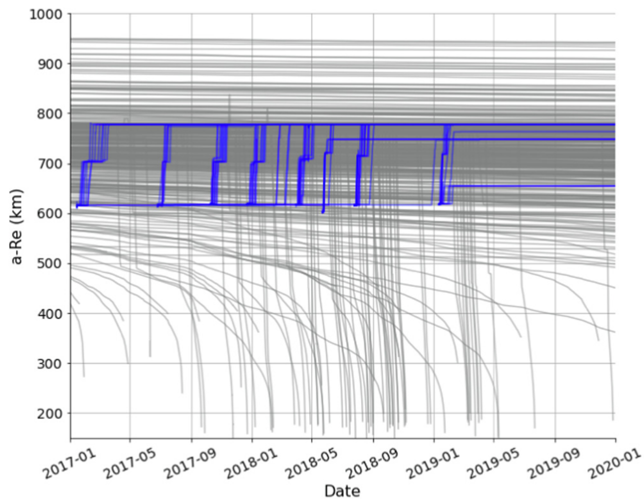

Fig. 2. Evolution of the semi-major axis of the Iridium satellites during the replenishment of the constellation. In gray the decommissioning of the first generation of satellites (Iridium) and in blue the deployment of the new generation (Iridium NEXT) carried up by 8 launches. (For interpretation of the references to colour in this figure legend, the reader is referred to the web version of this article.)

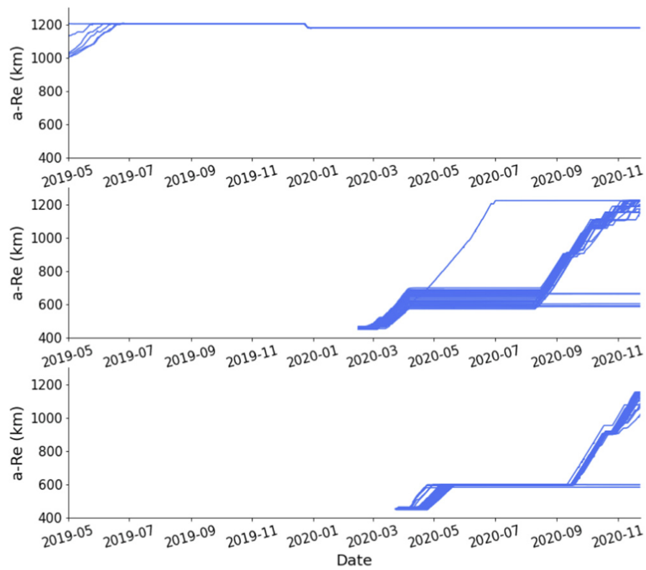

Fig. 3. Evolution of the semi-major axis of the first six OneWeb satellites launched at 1000 km of altitude on February 27, 2019, and 34 satellite at 450 km of altitude on February 6, 2020 and on March 21, 2020. The orbit raising has stopped in March and April 2020 after the bankruptcy of OneWeb on March 27, 2020.

2.1.2. OneWeb

The constellation OneWeb is the first announced project of large satellite constellation but in March 2020, the company announced the bankruptcy during the COVID crisis after the launch of 74 satellites. Initially, the constellation as scheduled will encompass 720 satellites operating at 1200 km of altitude, and distributed on 18 orbital planes, with 40 satellites in each orbital plane inclined at 87.9 degrees[4]. The first launch of a group of 6 test satellites occurred on February 27, 2019, on-board a Soyouz, and a second one occurred on February 6, 2020, with 36 satellites. In Fig. 3, the semi-major axis of OneWeb satellites are plotted showing the raising phase supported by their electric propulsion, performed after the injection at 1000 km of altitude for the first group test and at 500 km for the second group as for the next scheduled launches.

We note OneWeb proposed also a MEO constellation with 1280 satellites but not studied in this paper [5].

On May 26, 2020, OneWeb requested to the FCC the authorization to increase the number of satellite from 716 during a first phase to 47 844 during a second phase, all located at 1200 km of altitude but spread over three shells with 1764, 23 040, and 23 040 satellites whose orbital planes are inclined at 87.9, 40, and 55 degrees respectively[6].

The satellites, built by Airbus Defence and Space and Arianespace so far, have a mass of 147.5 kg, and a shape of 1 m × 1 m × 1.3 m.[7] They have an ion electric propulsion, a SPT-50 M's model of Fakel. In total 21 Soyuz or Ariane 6, and 39 Virgin Galactic launchers are to be used over a period of 2 years. A total of 588 satellites before the end of 2021 was expected to provide a full coverage. The decommissioning is envisaged performing an initial extraction by lowering the altitude to 1100 km, and later on, the perigee is lowered down to 250 km. Finally, the reentry should occur in less than 5 years.

The future of the OneWeb is still open. Even after the bankruptcy, OneWeb filled an application for 48,000 new satellites[8] and since July 2020 new investisors are now involved in the compagny.

2.1.3. Starlink

Starlink is a project of large constellation developed by Space X. It is the most ambitious project to provide a broadband internet connectivity over all the Earth surface. The initial project was to send 4425 satellite at between 1110 and 1325 km of altitude, spread over 83 orbital planes inclined between 53.8 and 70 degrees[9]. But 1,584 satellites initially planed at an altitude of 1150 km are lowered to 550 km with lower minimum Earth station elevation angle[10]. This choice will reduce the interaction with the region of highest space debris density and also with the Iridium constellation. Moreover, a second constellation will be placed in very low Earth orbit (VLEO), with a total of 7518 satellites between 335.9 and 345.6 km of altitude, at

[4] FCC file #SAT-LOI-20160428–00041, Technical attachment p.6.

[5] FCC file #SAT-AMD-20180104–00004, Technical attachment, p.1.

[6] FCC file #SAT-MPL-20200526–00062, Legal Narrative Attachment p.10.

[7] https://directory.eoportal.org/web/eoportal/satellite-missions/o/oneweb.

[8] FCC file #SAT-MPL-20200526–00062, See Attachment Legal Narrative p.1.

[9] FCC file #SAT-LOA-20161115–00118, of November 15, 2016. See Technical Attachment p.1.

[10] FCC file #SAT-MOD-20181108–00083 of November 8, 2018. See Technical Attachment p.3.

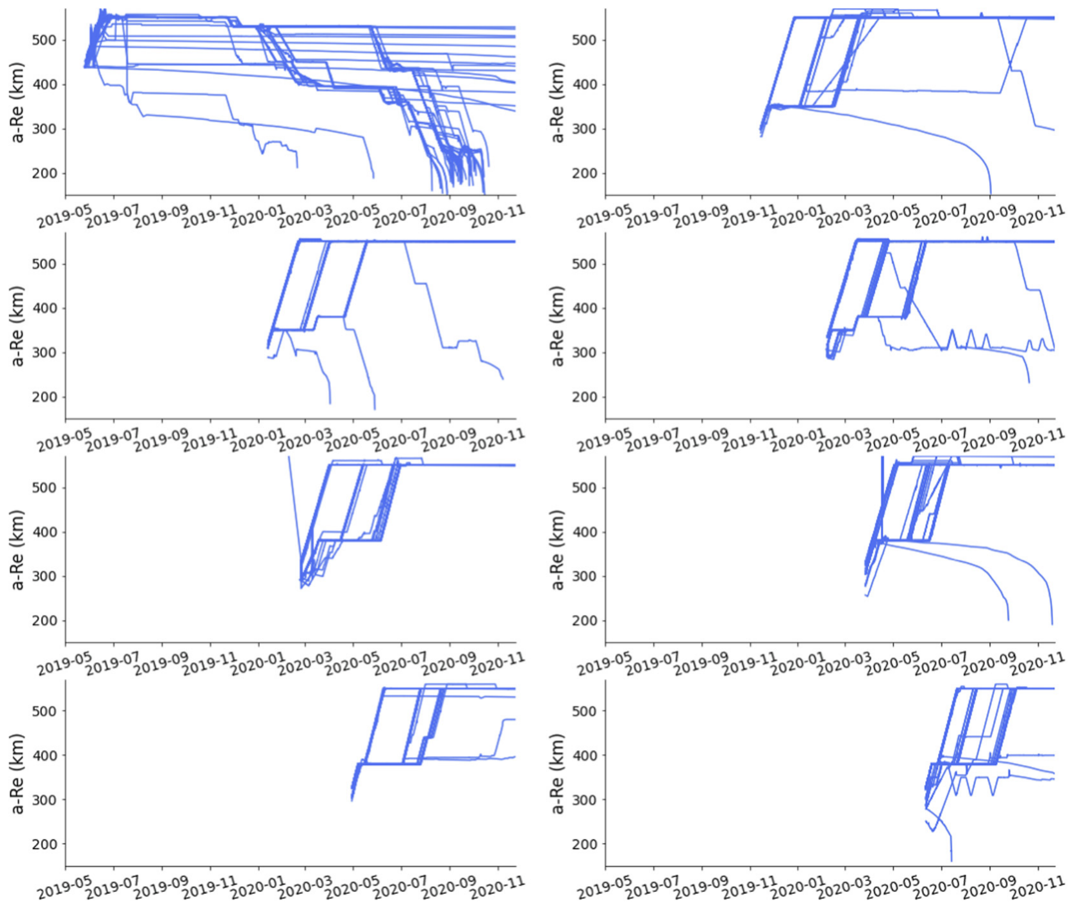

Fig. 4. Evolution of the semi-major axis of the Starlink satellites whose the first launching occurred on May 24, 2019. A total of 480 satellites has been launched between May 2019 and June 2020.

inclinations between 42 and 53 degrees[11]. We note that satellite above 1000 km of altitude are still scheduled. The period to launch the satellite is very short because the FCC imposes to launch half of the constellation in 6 years. An unprecedented launching rate will be necessary. On May 24, 2019, a first bunch of 60 satellites was launched. Since then, five new launches of 60 satellites occurred up to the date of March 18, 2020, and it will continue at the rate of 1 or 2 launches per month. After the first launch, Space X decided to modify the number of orbital planes at 550 km from 24 to 72 in order to provide sooner a service for American customers[12].

On May 2020, a last proposal was sent to the FCC for the application of 30,000 new satellites of a second generation between 328 and 614 km of altitude[13]. The complexity of the constellation increases with a panel of 8 altitudes with 1 or 12, 18 or 40 orbital planes, and inclinations from 30 up to 115.7 degrees. Moreover, if a majority of satellites are between 300 and 399 km of altitude where the collision probability is very low, the interaction with other satellites injected, and operating an orbit raising phase will be a major issue.

The satellites of first generation have a mass of 227 kg, with tabletop shape.[14] It was announced they are able to perform autonomous manoeuvres using a Hall thruster with xenon gas. As we can see in Fig. 4, the orbit insertion starts at 300–350 km of altitude and each satellite performs an orbit raising manoeuvre until 550 km of altitude[15]. The Starlink constellation is at the moment the largest constellation in orbit. However, a significant number of satellites launched did not reach their operational orbit (about 5%) due to system failures.

2.1.4. Kuiper

Amazon asked to the FCC an authorization to deploy a constellation providing a global Internet access like OneWeb and Starlink. The constellation is split in three parts: 784 satellites at 590 km of altitude, 1296 satellites at

[11] FCC file #SAT-LOA-20170301–00027 of August 2017. See Technical Attachment p.2.

[12] FCC file #SAT-MOD-20190830–00087, of August 30, 2019. See Technical Attachment p.2.

[13] FCC file #SAT-LOA-20200526–00055 of May 26, 2020. See Attachment Technical p.1.

[14] https://directory.eoportal.org/web/eoportal/satellite-missions/s/starlink.

[15] FCC file #SAT-MOD-20181108–00083 of May 26, 2018. See Attachment Technical p.42.

610 km, and 1156 satellites at 630 km, for a total of 3236 in the LEO region[16]. Inside each shell an in-track separation of 50 km is proposed. In a response of September 18, 2019 providing additional information, it is described that the injection of the satellites will be performed at an altitude below the ISS.[17] For the decommissioning, a 30-min burns, centered on the apogee, every orbit, will lower the perigee to 350 km in 95–130 days. Moreover, during the decommissioning phase, a specific strategy can be applied for collision avoidance manoeuvres. If a collision alert is received, then a manoeuvre lowers the apogee to modify the trajectory and to reduce the collision probability. The consequence is also a modification of the reentry date, sooner than the date scheduled without the manoeuvre.

2.1.5. Kepler

Kepler Communications will deploy a constellation of 140 small satellites (3U CubeSats), in 7 orbital planes, on Sun-synchronous polar orbits at 575 km of altitude to provide a service for Internet-of-things[18]. The company expects a deployment in three years from 2020 to 2022. The first launch is scheduled on-board a Falcon 9 for a total payload of 400 kg. As we expect 15 satellites for the first launch we assume a mass of 27 kg for each satellite.

A new request have been performed to extend the constellation up to 360 small satellites dispersed in 12 near-polar orbital planes[19]. For the decommissioning, the satellites perform manoeuvres during 27 days to decrease the altitude from a operational maximum of 650 km to 300 km on a circular orbit.

2.1.6. Telesat

Telesat proposed an initial LEO constellation with 117 satellites split in polar and inclined constellations. It was recently modified to contain a total of 1671 satellites. Now, it foresees 351 satellites at 1015 km of altitude in 27 polar orbital planes inclined at 99.5 degrees, and 1320 satellites at 1325 km of altitude in 40 orbital planes inclined at 50.88 degrees [20]. The FCC has already accepted the launching of 117 satellites and the global service starting is scheduled for 2022. The first launch is scheduled in 2021–2022 and an agreement have been signed between Telesat and Blue Origin for launches with the New Glenn, which will be able to carry up to 45 metric tons to LEO.

[16] FCC files #SAT-LOA-20190704–00057 on July 04, 2019. See Attachment Technical p.2.

[17] https://licensing.fcc.gov/myibfs/download.do?attachment_key=1912531.

[18] FCC files #SAT-PDR-20161115–00114 on November 15, 2016. See Attachment Legal Narrative p.5.

[19] FCC files #SAT-LOA-20200526–00059 on July 04, 2019. See Attachment Exhibit B p.2.

[20] FCC file #SAT-MPL-20200526–00053 of May 26, 2020. See Attachment Technical p.3.

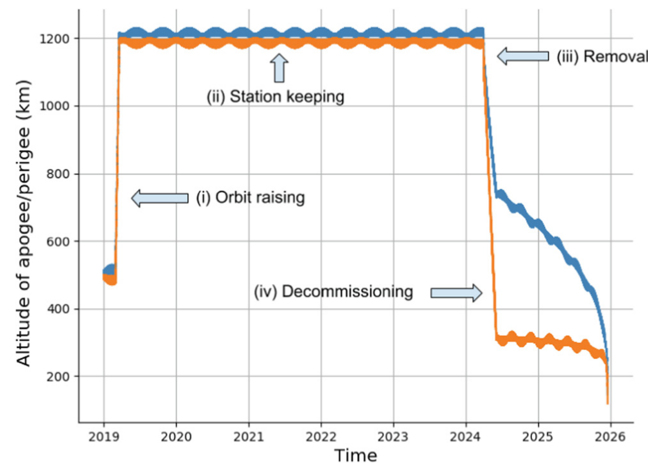

Fig. 5. Apogee and perigee of a OneWeb satellite during the whole orbital life. We identify four phases: (i) the orbit raising, (ii) the operational phase, (iii) the removal from the constellation and the lowering of the perigee, (iv) and the atmospheric reentry.

3. Orbital manoeuvres

3.1. Orbit propagation from injection to decommissioning

The satellites are placed in orbit in groups of 10 satellites (OneWeb) or 60 (Starlink) by a same launcher. They are injected in a low orbit and they have to use their own propulsion to raise their orbit and to reach the operational altitude. The new generations of satellites use an electrical propulsion system providing a low thrust. It allows to increase the altitude with a low constant acceleration directed along the velocity direction. For decommissioning, the perigee is lowered.

For the purpose of our study, the ephemeris of a satellite is obtained by numerical propagation. The numerical integrator is based on the Shampine-Gordon method (Shampine and Gordon, 1975), the dynamical model is a singly-averaged formulation on Keplerian orbital elements, accounting for the following effects:

- zonal harmonics $J_2 - J_3 - J_4 - J_5$;
- the effect due to atmospheric drag only on eccentricity and semi-major axis, given the Jacchia-Roberts atmospheric density model assuming an exospheric temperature of 1000 K and a variable solar flux at 2800 MHz;
- solar radiation pressure (cannonball model coupled with the oblateness effect (Alessi et al., 2018));
- lunisolar gravitational perturbations, using analytical ephemerides for Sun and Moon (Simon et al., 1994).

Moreover, the phase of orbit raising is modeled using a formulation of the long-term variation of the orbital elements due to an acceleration tangent to the orbit path (Pollard, 1997). For the decommissioning phase, we adopt a de-orbit strategy consisting of lowering the perigee, and to achieve a passive reentry supported by atmospheric drag (Huang et al., 2019). In Fig. 5, the apogee and perigee are plotted for a OneWeb satellite during the whole orbital life. In Table 2, we summarise the characteristics of the initial orbit before the orbit raising phase, and the decommissioning orbit.

3.2. Lifetime and failure case

It has been shown that the orbital lifetime after the operational phase is one of the most important parameters to ensure the sustainability of the space environment (Virgili et al., 2016; Lewis et al., 2017). Thus, we assess the residual lifetime of the satellite for different cases: (i) after a failure in the orbital injection, (ii) after a failure on the operational orbit, (iii) after the decommissioning manoeuvre lowering the perigee. Moreover, as the intensity of the solar activity affects the atmospheric drag and thus, the reentry date, we consider a low and a strong solar activity. The future solar activity cannot be predicted on the long-term period in the future. However, we can model a realistic scenario fitting the historical data of the mean solar radio flux by a Fourier polynomial as described in (Petit and Lemaitre, 2016). In order to obtain a scenario with a low solar activity or a high solar activity, we lower or we increase respectively the values by 10%, keeping a minimal value at 75. In Fig. 6, the solar activity is plotted for both scenarios.

The propagation is performed using the information in the Table 2 and Table 3. The lifetimes are given in Table 4. These values of lifetime are sensitive to parameters like the ballistic coefficient (which depends on the mass, shape and orientation of the satellite) and the solar activity. But as a first approximation, we observe that due to orbit injections at a low altitude the lifetime in case of initial failure is reduced to about one year. A failure on the operational orbit for a Kuiper or Starlink satellite leads to stay about one decade in orbit but it is still less than the 25-years rule recommended. However, for a OneWeb satellite, if a failure occurred, the atmospheric drag does not act and the satellite first drift inside the orbital plane towards other satellites, and second, towards other orbital planes, leading to conjunctions and in the worst case a collision (Rossi et al., 2020). Then without removal action, the constellation operation will be disrupted.

4. Method to assess the close approach frequency and the cumulative collision probability

We propose a software to assess the long-term collision risk in terms of close approach frequency and collision probability between a target satellite and the background environment of space debris by a Monte Carlo process. It is based on the CUBE algorithm used as a filter for conjunction and the Foster method in case of close approach to calculate the collision probability taking into account assumptions about the data uncertainty. We introduce the method and the statistics inferred like the number of

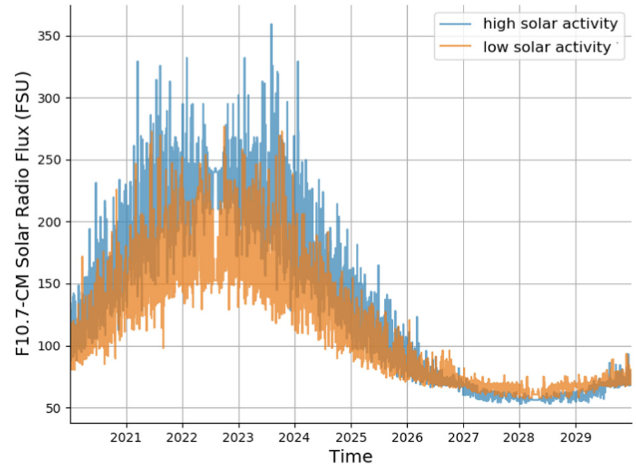

Fig. 6. Models of low and high solar activity for the next decade used for the orbit propagation.

Table 3
Physical characteristics of the satellite OneWeb, Starlink and Kuiper. The sources are given in Section 2. As the exact orientation of the solar panels are not known, we assumed a cross-section area following Lewis et al. (2019). The design of Kuiper satellite is still unknown but it will probably be similar to Starlink satellites. (*: assumed value).

Name	OneWeb	Starlink	Kuiper
Mass of the target [kg]	147.5	227	227*
Cross-section area of the target [m^2]	3.5*	3.5*	3.5*

Table 4
Lifetime in days of the satellite before the atmospheric reentry. Scenario 1: failure after the injection. Scenario 2: failure on the operational orbit. Scenario 3: lifetime on the decommissioning orbit. For each case an estimation is given for a low and high solar activity respectively the first and second value.

Name	Scenario 1	Scenario 2	Scenario 3
OneWeb	1008/850	–/–	113/133
Starlink	155/147	3694/686	127/162
Kuiper	108/108	4170/815	433/300

Table 2
Apogee/perigee or altitude of injection, operational altitude, and apogee/perigee of the decommissioning orbit for the satellite constellations OneWeb, Starlink, and Kuiper. These values are given by the FCC files introduced in the Section 2

Name	Injection (km)	Operational altitude (km)	Decommissioning (km)
OneWeb	500	1200	1100 × 250
Starlink	370 × 210	550	550 × 300
Kuiper	350	590/610/630	590/610/630 × 350

conjunctions and the cumulative collision probability. Moreover, we provide some comments about the parameters used.

4.1. Detection of close approaches and computation of the collision probability

The CUBE algorithm was developed at NASA/JSC (Liou, 2006). It allows to detect close approaches in a population of space objects performing a uniform sampling of the circumterrestrial system in time and space. The original idea is to express the cumulative collision probability between two objects i and j over a period of time

$$P_{i,j} = \int_{t_{begin}}^{t_{end}} P_{i,j}(t)dt = \int_{s=0}^{s=L} [t_{s+1} - t_s]P_{i,j}(s)\mathrm{d}s \quad (1)$$

where $P_{i,j}(t)$ is the collision probability between the object i and j at the epoch t, L is the number of time intervals between t_{begin} and t_{end}, and t_s the date of the interval s. At each epoch s of the interval we compute a snapshot of the target and the population, and we apply the following steps:

- First, we perform a comparison between apogee and perigee of the target and each object of the background population in order to exclude a conjunction possibility in a low computation time.
- Second, we discretize the tridimensional space in small cubes with a typical size of 10 km $\times$ 10 km $\times$ 10 km.
- If two objects are in the same cube, then we have a potential conjunction event and we compute the collision probability $P_{i,j}(s)$.

Once two or more objects are found within the same cube, in the standard CUBE method, the collision probability is computed by means of the particle-in-the-box equation. For our purpose, we use a more accurate method based on the assumption of a Gaussian distribution of the position and as we focus on the LEO region, we expect fast encounters. We adopt the Foster method, used by the National Aeronautics and Space Administration (NASA) to compute the on-orbit collision probability for the ISS, the Space Shuttle, and now generally used to asses the accurate the collision probability in case of close approach. The complete formulation of the method is given in Klinkrad (2006).

In our software, when two objects are in the same cube, we save the Cartesian coordinates and we propagate both objects until the time of closest approach (t_{ca}). We assume that the target and chaser bodies are spheres, and that the covariance matrices are uncorrelated. They are summed and projected on the encounter plane (or B-plane) allowing to integrate numerically the two-dimensional Gaussian probability density function (pdf) (Alessi et al., 2014).

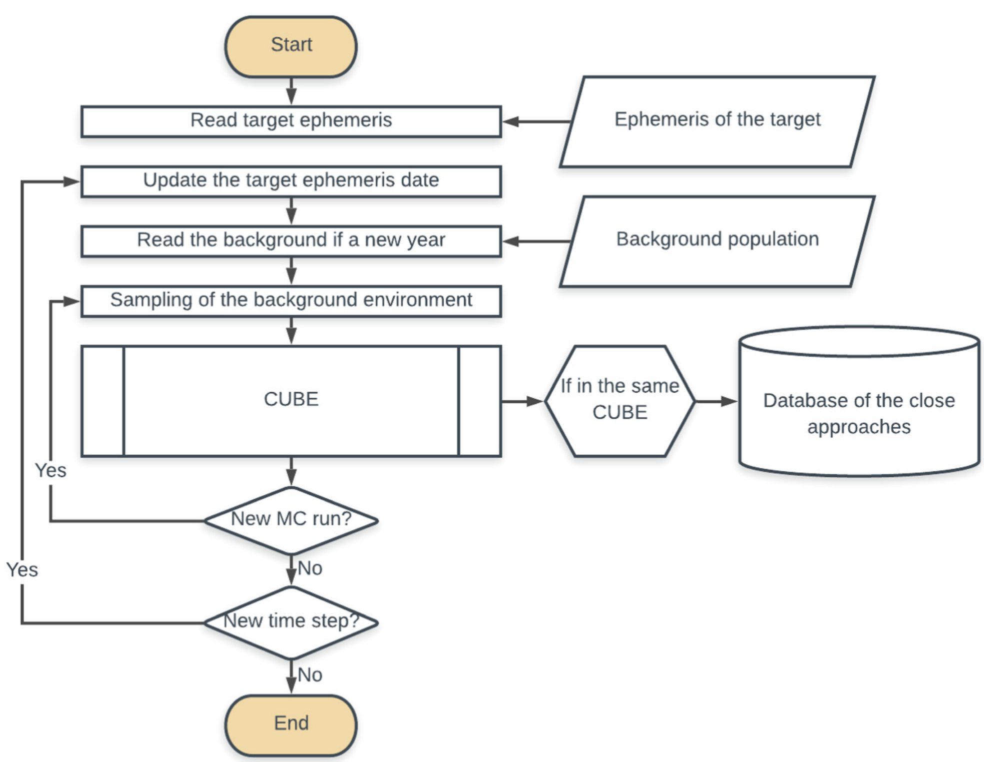

Fig. 7. Flowchart to assess the close approach frequency and the cumulative collision probability during the orbital life of a satellite. The CUBE algorithm is used as a close approach filter filling a realistic event database for an individual satellite.

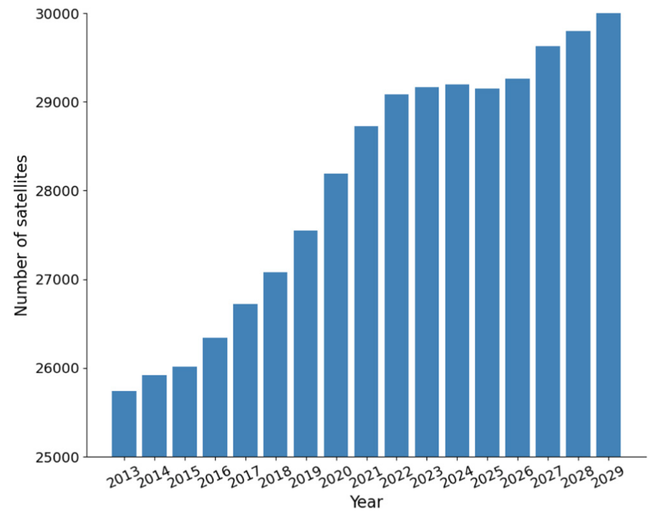

Fig. 8. Evolution of the number of resident space objects (RSO) with a size larger than 10 cm simulated with SDM.

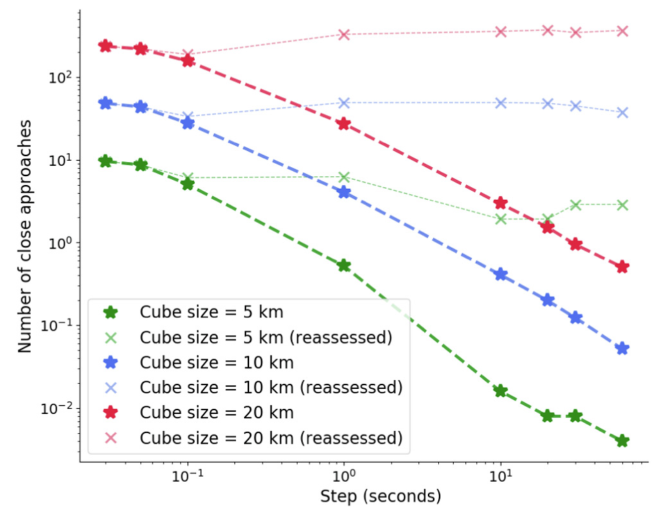

Fig. 9. Benchmark of the CUBE algorithm for the cube size and time step. The total number of close approaches detected, i.e. each time an object of the background environment is detected in a same cube with the target satellite, is given as a function of the time step. We observe a plateau for time step inferior to 0.05 s. The crosses are the same values reassessed by the Eq. (2) (i.e. multiplied by a factor $12\Delta t$ being Δt the time step in seconds).

In Fig. 7, we provide the flowchart of the software. It takes as inputs the ephemeris of the target satellite and snapshots of the space debris background environment at the beginning of each year, as described in the next subsection. The software returns a set of close approaches defined by the epoch, the Cartesian coordinates of the target and chaser object, the position standard deviations (the error on the velocity is negligible), areas and masses, and the collision probability computed. The analysis of the database allows to assess the characteristics of the close approaches during the lifetime of the satellite, as well as the cumulative collision probability, and the occurrences of potential collision avoidance manoeuvres.

4.2. The space debris population

The software uses a background space debris environment produced by evolving in time an initial population of objects larger than 10 cm, extracted from the ESA MASTER population (Flegel et al., 2009). The long-term evolution is performed by means of the SDM model considering a reference scenario where launches, in-orbit explosions (2–3 per year until 2028) and collisions are considered (Rossi et al., 2009). A repeating launch traffic, based on launches as between 2005 and 2012, is considered (it is the standard traffic launch used in most of the IADC comparative studies so far Committee et al., 2013). Note that for the kind of analysis performed here any slight change in background traffic launch would have a very limited effect. A variable $F_{10.7}$ solar flux, with mean value around 115 units is used Schaus et al. (2017),Lewis et al. (2017). All the active objects are supposed to perform collision avoidance maneuvers with an 80 % success rate. Moreover, each spacecraft that does not naturally comply with the 25-year rule, is performing a post-mission disposal maneuver with a success rate of 60 %. This population of objects is evolved off-line, i.e., without the inclusion of the large constellations mentioned above, with 50 Monte Carlo (MC) runs. The output of the whole set of 50 MC runs is stored at fixed time steps. It is, later on, read by the constellation analysis software and used as a background against which to evolve the constellation satellites. In Fig. 8, the time evolution of the background population of objects larger than 10 cm is shown for 20 years.

4.3. Benchmark of the algorithm

The choice of the time and space sampling drives the detection of the close approaches as it was shown in (Blake and Lewis, 2014). The typical size of 10 km for the space sampling in cubes is equal to the significant distance of a close approach. Above 10 km the collision probability is negligible assuming a position uncertainty up to 1 km. However, in LEO the relative velocity is about 10 $\mathrm{km\,s^{-1}}$. Then, the time sampling to detect all close approaches is inferior to one second. Then, the final value of the cumulative collision probability and the detection of a maximal number of close approaches will depend on the frequency of the snapshots, but the detection of conjunctions between a target and several thousand of objects is time consuming.

To assess a compromise between computational time and accuracy we performed a benchmark of the CUBE algorithm results using a Starlink satellite over a period of one day. We vary the cube size and the time step. In Figs. 9 and 10 the total number of close approaches and the cumulative collision probability are plotted taking as cube size 5, 10 and 20 km, and as time step values 60, 30, 20, 10, 5, 1, 0.1, 0.05 and 0.03 s, over a time span of one day. In order to avoid a double recording of the same individual close approach, a screening is performed. We

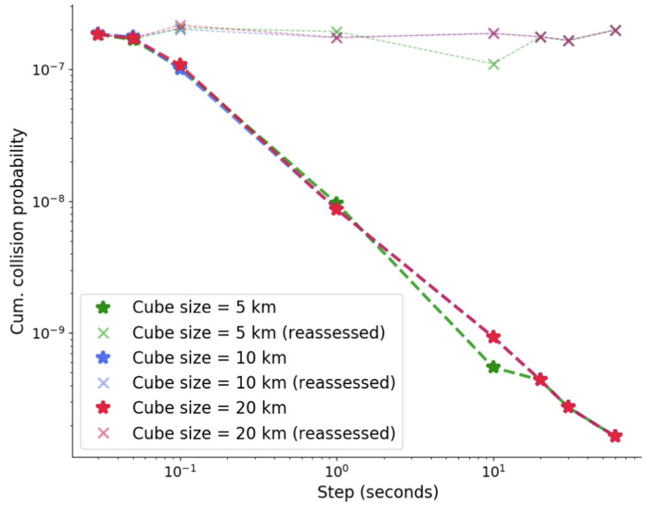

Fig. 10. Benchmark of the CUBE algorithm for the cube size and time step. The cumulative collision probability is given as a function of the time step. We observe a plateau for time step inferior to 0.05 s. Moreover, if we increase the size of the cubes, the miss distance of additional objects detected is larger and the collision probability negligible. The crosses are the same values reassessed by the Eq. (2) (i.e. multiplied by the factor $12\Delta t$ with Δt the time step in seconds).

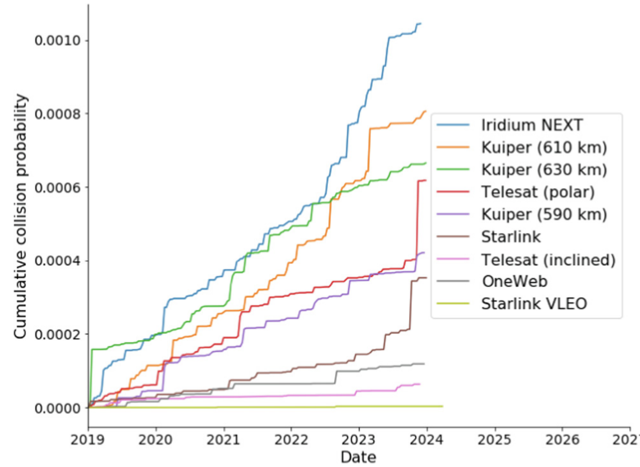

Fig. 11. Cumulative collision probability for individual satellites of each large constellation. We assume a position uncertainty of $200 \times 1000 \times 300$ m along the radial, in-track, and cross-track directions for the target satellite and the objects of the background environment.

observe a linear relation between the time step and the number of close approaches detected. Divided by two the time step leads to double the number of close approaches but we observe that trend stops at about 0.05–0.03 s. Therefore, for our specific purposes, on the basis of the results shown in Figs. 9 and 10 the Eq. (1) can be rewritten

$$P_{i,j} = 12\Delta t \int_{s=0}^{s=L} P_{i,j}(s)\mathrm{d}s \tag{2}$$

with Δt the time step in seconds, to obtain an absolute estimation of the close approaches and cumulative collision probability. Considering a mean relative velocity equal to 8.6 km.s^{-1} between the target and chaser objects during close approaches, the characteristic time passed by two objects in a same cube of 10 km is 0.1–0.05 s in agreement with the plateau in Figs. 9 and 10. The reassessed values obtained with the Eq. (2) are also plotted. The new values are independents of the time step.

Moreover, if we increase the cube size then the number of close approaches increases too but the cumulative collision probability is pretty similar for a cube size of 10 or 20 km (see Fig. 10). The contribution of close approaches with a relative distance superior to 10 km is negligible.

5. Applications

In this Section, we apply our algorithm to obtain statistics about close approaches for satellites in different constellation configurations taking into account the evolution of the background environment of space debris. First, we focus on the operational altitude over a period of 5 years. Second, we focus on the variations during the different phases of the mission from the orbit raising to the decommissioning.

5.1. Relative and absolute close approach statistics

We compare the level of risk, i.e. the close approach rate and the cumulative collision probability, over a period of five years, at the altitudes and inclinations given for each constellation in Table 1. We obtain the relative number of conjunctions during this period and the cumulative collision probability following the algorithm introduced in Section 4 with a given time step, and using the ephemeris typical of a satellite inside each constellation, i.e. with the same initial semi-major axis, eccentricity and inclination although the right ascension of the ascending node, the argument of the perigee and mean anomaly are randomly chosen. Moreover, taking into account the considerations of the benchmark in subSection 4.3, we propose an assessment of the absolute cumulative collision probability. For this purpose, we use our software taking as parameters a cube size of 10 km and a time step of 300 s. To assess an absolute value we use the Eq. (2) that gives the cumulative collision probability assuming a linear relation of the final value with the time step (there we use the factor $12\Delta t = 3600$). The position standard deviation is $200 \times 1000 \times 300$ m in the local satellite frame for the target satellites Klinkrad (2006) and the objects of the background environment which is the typical uncertainty of TLE, and the cross-section of the target satellite is equal to 3.5 m^2 which is the value used in (Lewis et al., 2019). These assumptions provide a first comparison of the risk as previously defined but we keep in mind that an extended study has to be performed to assess the infuence of different values of covariance and cross-section.

The process is applied for ephemerides similar to an individual OneWeb, Starlink, Kuiper, Telesat and Kepler

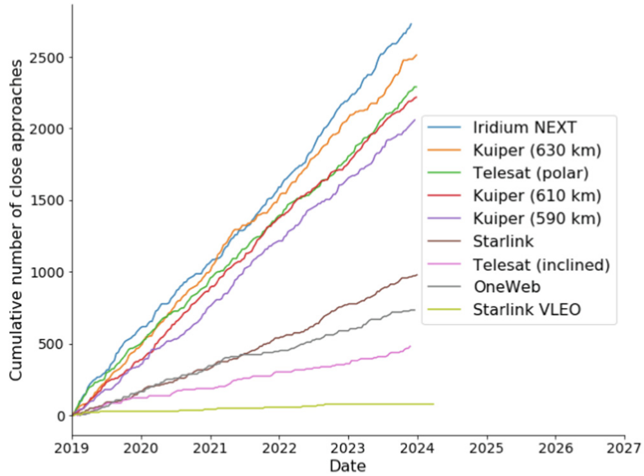

Fig. 12. Cumulative number of close approachess (< 4 km) for individual satellites of each large constellation.

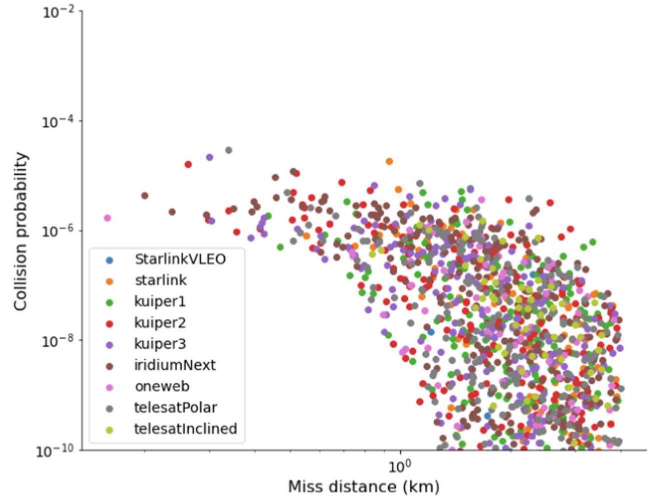

Fig. 13. Distribution of the collision probability for the close approaches (< 4 km) in function of the miss distance.

satellites on their nominal altitude. Then in Fig. 11, the evolution of the cumulative collision probability for an individual satellite of each constellation is plotted. It evolves with the changes of the background environment. The second shell of the Kuiper constellation (located at 610 km) has the highest cumulative collision probability followed by the two other shells (respectively located at 590 and 630 km). One order of magnitude below we have the Starlink and OneWeb constellations (respectively at 550 km and 1200 km). In Fig. 12 the evolution of the cumulative number of close approaches with a miss distance below 4 km is plotted. The three shells of the Kuiper constellation and the shell of Telesat with satellites on polar orbits have a higher rate of close approaches. These results are in agreement with Fig. 1 giving the density at the different altitudes and showing the Kuiper constellation in a region of high density.

In Table 5, we report the cumulative collision probability for an individual satellite of each large constellation after 5 years on their nominal orbits. These values are an absolute estimation taking into account the consideration of the subSection 4.3. We recall that if the CUBE algorithm is used with a time step of 300 s, we retrieve the absolute assessment multiplying the results by a factor 6000. Moreover, only close approaches with a collision probability higher than 10^{-8} have a significant contribution to the risk level and as we can see in Fig. 13 where the distribution of the collision probability in function of the miss distance is plotted. Hence, only close approaches with a miss distance below 4 km are involved. Thus, we report the total number of close approaches under theses conditions and their frequency over one day.

We recall that our software saves the dynamical state of the target and the chaser at each conjunction. In order to characterize the populations involved, in Figs. 14–16 the distributions of the semi-major axis, the eccentricities, and inclinations of these objects at the time of closest approach are plotted. First of all, the objects have a semi-major axis close to the semi-major axis of the constellation concerned and an eccentricity inferior to 10^{-1}. For OneWeb and Telesat, the two constellations at the

Table 5
Cumulative collision probability for one individual satellite and for the full constellation assuming a position uncertainty of 200 × 1000 × 300 m along the radial, in-track, and cross-track directions for the target satellite and the objects of the background environment.

Name	$P_c^{cum,1sat}$	Close approaches (<4 km)	Frequency (day^{-1})
Starlink VLEO	$3.40 \cdot 10^{-5}$	864	0.47
Starlink	$3.53 \cdot 10^{-3}$	9864	5.40
Kepler	$1.81 \cdot 10^{-3}$	9000	4.93
Kuiper (590 km)	$4.21 \cdot 10^{-3}$	20 664	11.32
Kuiper (610 km)	$8.08 \cdot 10^{-3}$	22 248	12.19
Kuiper (620 km)	$6.65 \cdot 10^{-3}$	25 200	13.8
Iridium NEXT	$1.05 \cdot 10^{-2}$	27 432	15.03
Telesat (polar)	$6.17 \cdot 10^{-3}$	23 040	12.62
OneWeb	$1.20 \cdot 10^{-3}$	7488	4.11
Telesat (inclined)	$6.36 \cdot 10^{-4}$	4896	2.68

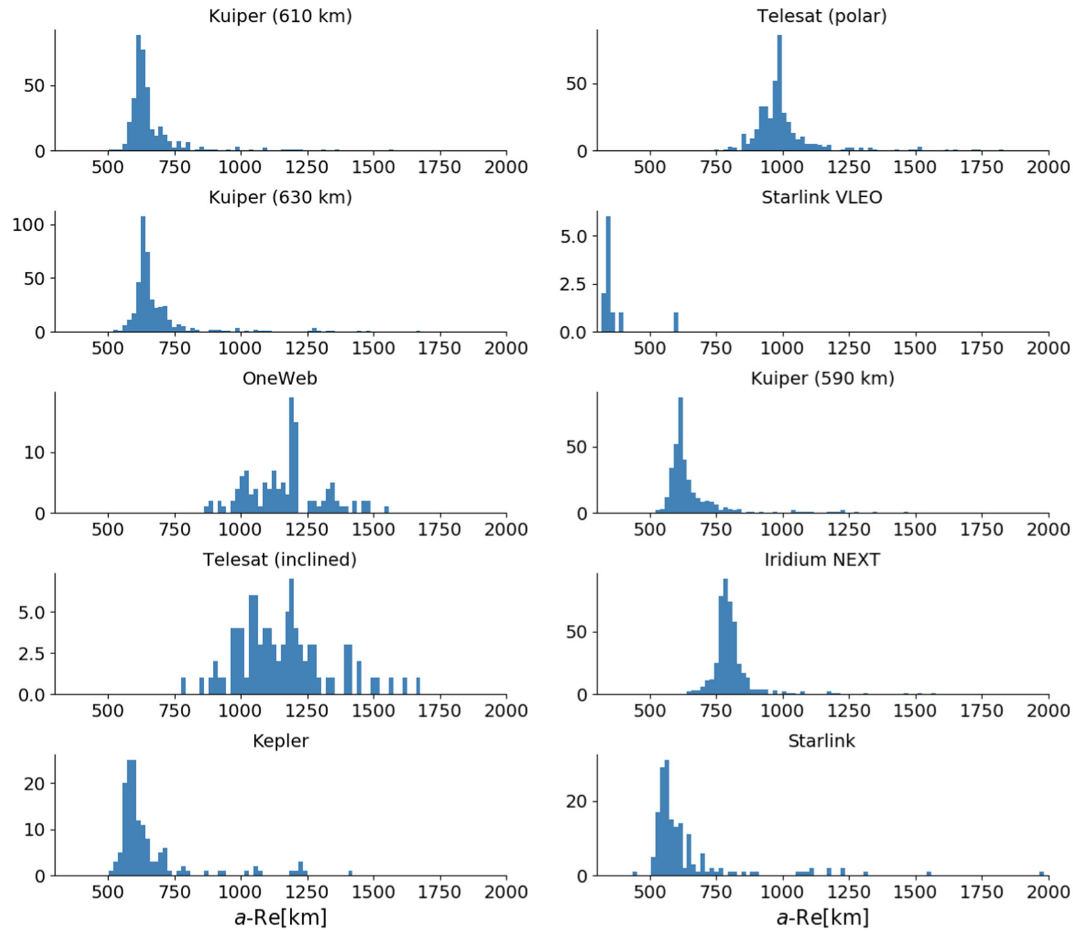

Fig. 14. Semi-major axis distribution of the objects of the background environment involved in a close approach.

highest altitudes, while a smaller population is involved in the conjunctions, it spreads on the larger range of the semi-major axis between 800 and 1400 km of altitude. Indeed, the constellation being in higher orbits can interact with objects with a significant eccentricity and a lifetime enough to enter in the statistics. In inclination, a majority of objects has an inclination close to 98 degrees (the Sun-synchronous orbit), 85 degrees and 65 degrees. For Starlink, Kuiper and Kepler, the most problematic population comes from the Sun-synchronous orbit, which is mainly filled by the fragments of the Fengyun 1C satellites.

5.2. Complete operational life

A more detailed investigation can be performed for the large constellations whose design is well defined like OneWeb and Starlink. In Fig. 17 the evolution of the cumulative collision probability and the evolution of the semi-major axis are plotted to highlight the different phases of the orbital life of the satellite considering the deployment with orbit raising, the station-keeping during the operational phase, and the decommissioning until the atmospheric reentry. As in the previous section, the CUBE algorithm is applied using the ephemerides similar to a OneWeb and a Starlink satellite from orbit raising to the decommissioning and reentry. The time step is 300 s and the position standard deviation is $200 \times 1000 \times 300$ m in the local satellite frame for both target satellites and the objects of the background environment. On the top the case of OneWeb is plotted: during the orbit raising and the decommissioning phase the satellite crosses crowded regions and the largest increases of the cumulative collision probability are seen during these phases. On the lower plot the case of Starlink is plotted: the collision probability during these first and last phases is negligible. In Table 6, we give the ratio of the cumulative collision probability between each phases (i.e. the cumulative probability during a phase divided by the total cumulative collision probability). For OneWeb, the decommissioning is a critical period because it represents 13.28 % of the cumulative collision probability. In (Radtke et al., 2017), a similar study was performed for a OneWeb satellite. They found the decommissioning phase has the highest collision probability. The main reason is the reentry time which is about five years in the paper and three years in our simulation. Then it is clear that the decommissioning phase of the OneWeb satellites will be critical because an extension of the reentry duration

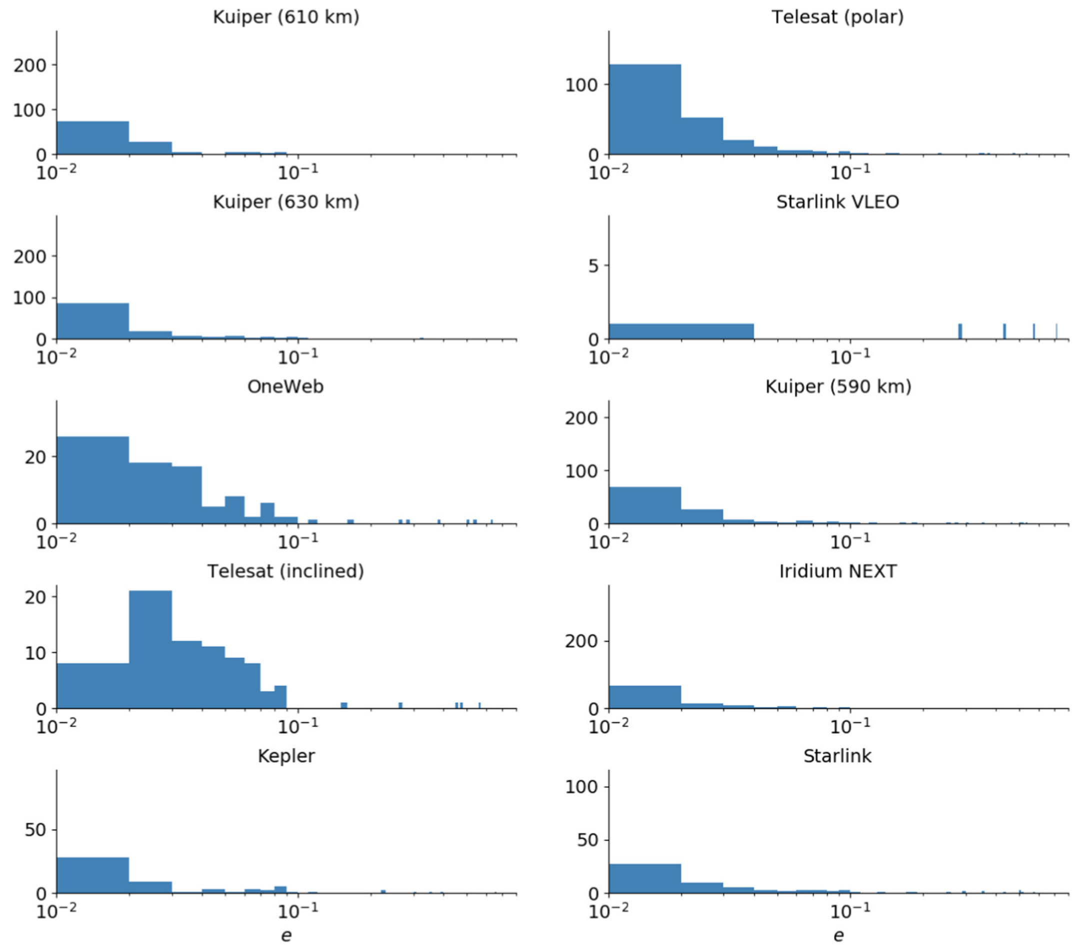

Fig. 15. Eccentricity distribution of the objects of the background environment involved in a close approach.

will increase the collision risk, and the additional costs arising from the collision avoidance management have to be taken into account. For a Starlink satellite, because of the orbit raising and decommissioning phases are below altitudes with high space debris density, the ratios is marginal.

Conclusions about Starlink can be extended for a Kuiper or Kepler satellite because their nominal altitudes are very close (respectively 575 to 630 km). In case of satellite failure, Space X claims a collision probability $6.2 \cdot 10^{-8}$ at 328 km, and $2.867 \cdot 10^{-4}$ at 614 km until the natural atmospheric reentry. But without precise information about the cross-section or the duration of the reentry the results are hard to compare.

Note that, for each considered constellation, the simulations are performed considering a background population not including the other large constellations. The interaction between the different constellations is not included (since the situation is still so uncertain) but clearly their presence will increase the complexity of the navigation, even if we can expect a coordination between operators.

We investigate the sensibility of the collision probability to the duration of the different phases. The magnitude of the low-thrust will change the duration of the orbit transfer, and thus the collision probability. In Tables 7 and 8 for the OneWeb and Starlink satellites respectively, we report the time span of the orbit raising for different values of the tangential thrust applied, the number of conjunctions and the cumulative collision probability computed over this period. The magnitudes of the low-thrust provide duration in agreement with the transfer observed in Fig. 3 and 4. For the Starlink satellite, the risk stays very low, even with a long transfer, because the regions between 300 and 550 km are not as congested in comparison.

Finally, we assess the collision probability during the decommissioning as described in the scenario 3 of the Table 5. In Table 9, we report the duration of the disposal, the cumulative collision probability during this phase, and the number of conjunctions for the cases of low and high solar activity. A high solar activity reduces the lifetime of the satellite and thus the collision probability which stays above 10^{-4} as shown by Space X and Kuiper. Again, for a OneWeb satellite the collision probability is higher than that for a Starlink satellite because during a long part of this phase, it orbits at altitudes between 300 and 700 km as shown in Fig. 17.

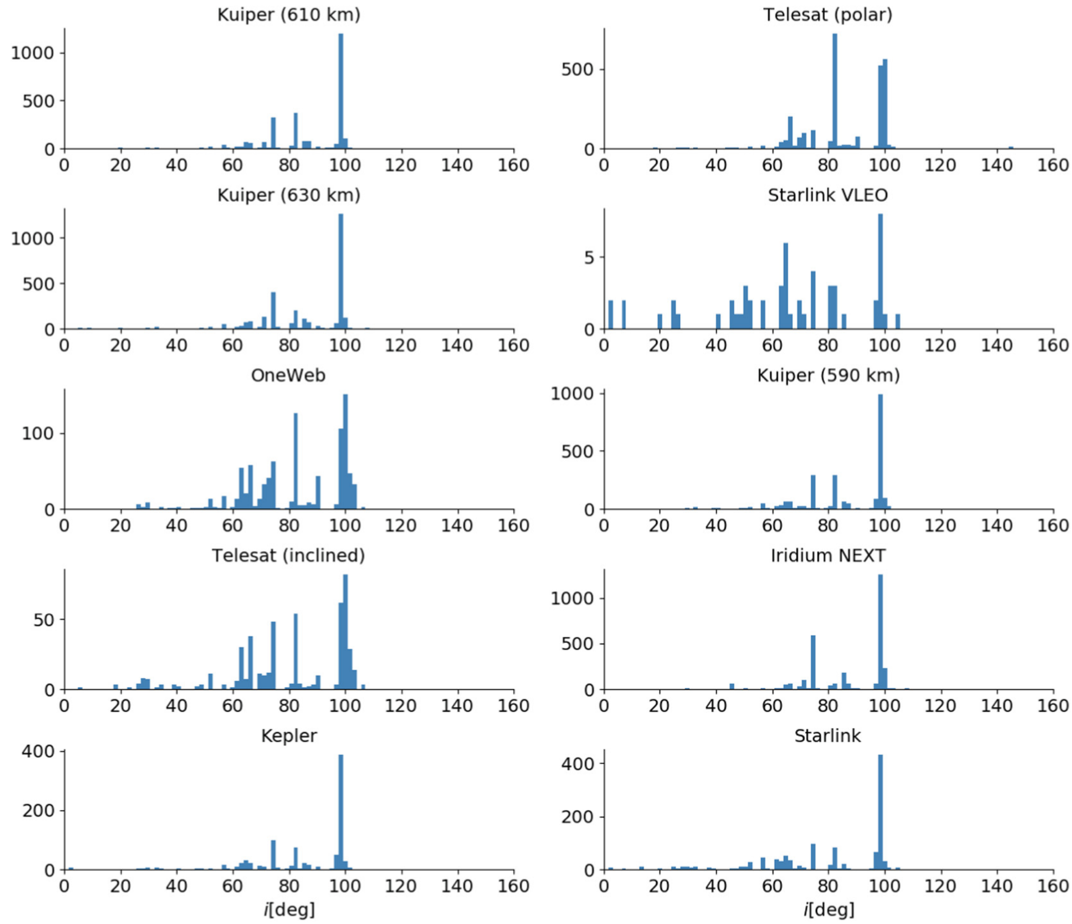

Fig. 16. Inclination distribution of the objects of the background environment involved in a close approach.

6. Conclusions

Considering the intensification of the space activity related to the advent of large constellations, the assessment of the collision probability in this new context is a priority. We propose to assess the collision probability using an alternative approach to other works (May et al., 2018; Radtke et al., 2017). We implemented the CUBE algorithm to detect conjunctions of a satellite with a background environment of space debris and we use the Foster method to compute the collision probability with the assumption of the uncertainty in position. Moreover, this software fills a database of close approaches allowing in future work to study collision avoidance strategies.

For the large satellite constellations Iridium Next, OneWeb, Starlink, Kuiper, Telesat, and Kepler we provide the close approach rate and the cumulative collision probability. The satellites of the constellations Iridium Next, Kuiper and Telesat have the higher cumulative collision probability with Starlink and Kepler just below. However, we note that the very large number of satellites inside the constellations Starlink and Kuiper will overwhelm the space traffic creating a very important number of conjunction alerts. For Kuiper, the assessment results in 11–13 close approaches with miss distance below 4 km per day, and 5–6 for Starlink.

It was shown that the decommissioning phase contribute for a non-negligible part to the global risk for the OneWeb satellites because satellites they cross crowded regions although the risk is negligible for the Starlink satellites that are at a lower altitude. We note that our future studies will investigate the interaction between constellations, in particular during each orbit raising and decommissioning. In particular, Kuiper satellites will cross the Starlink constellation at a very high rate during to the deployment and replenishment process. It will be a challenge for the space traffic management in terms of coordination between the different actors. For instance we need more transparency sharing ephemerides and manoeuvres planned, and voluntariness to avoid conflicts and keep a fair use of space.

These results will be soon compared with the databases of conjunction data messages received in real conditions for the first satellites already launched. It is also worth noting that the deployment of the Starlink constellations and cubesats are already changing the overall distribution of objects in LEO, increasing the density of objects in very low orbits previously almost unpopulated.

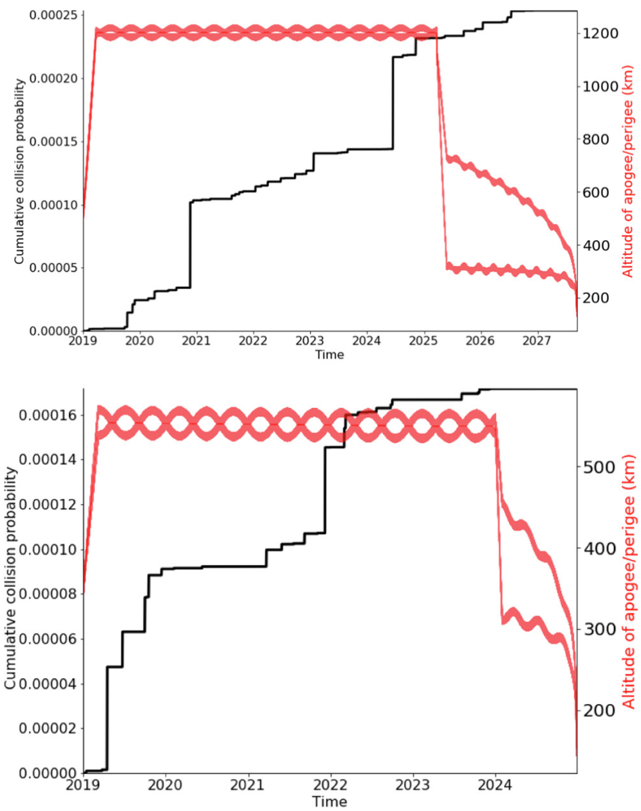

Fig. 17. The evolution of the perigee and apogee are plotted in red for a OneWeb (top) and a Starlink (bottom) satellite. The satellites perform the orbit raising, station-keeping maneuvers during 5 years, and decommissioning maneuvers lowering the perigee towards an atmospheric reentry. The evolution of the cumulative collision probability obtained with our implementation of the CUBE algorithm is plotted in black. Note that values are obtained with a time step of 300 s and a constant position standard deviation of 200 × 1000 × 300 m in the satellite local frame for the computation of the collision probability. (For interpretation of the references to colour in this figure legend, the reader is referred to the web version of this article.)

Table 6
Ratio of the cumulative collision probability for each phase, i.e. the orbit raising, station-keeping and decommissioning phases for a satellite of the OneWeb and Starlink constellation.

Phase	OneWeb (%)	Starlink (%)
Orbit raising	0.01	≈ 0.54
Station-keeping	86.71	99.41
Decommissioning	13.28	≈ 0.05

Table 7
Number of conjunctions and cumulative collision probability for a OneWeb satellite during different time spans of the orbit raising phase which depend on the tangential thrust applied after the injection at an altitude of 500 km as described in Section 2 and 3.

Thrust ($m.s^{-2}$)	Time span (day)	$P_c^{cum,1sat}$	Conjunctions (<10 km)	Conjunctions (<1 km)
$1 \cdot 10^{-4}$	42	$4.28 \cdot 10^{-7}$	3479	6
$5 \cdot 10^{-5}$	83	$2.37 \cdot 10^{-4}$	7560	120
$2 \cdot 10^{-5}$	208	$7.45 \cdot 10^{-3}$	20 260	240

Table 8
Number of conjunctions and cumulative collision probability for a Starlink satellite during different time spans of the orbit raising phase which depend on the tangential thrust applied after the injection at an apogee at 370 km of altitude and a perigee at 210 km as described in Section 2 and 3.

Thrust ($m.s^{-2}$)	Time span (day)	$P_c^{cum,1sat}$	Conjunctions (<10 km)	Conjunctions (<1 km)
$1 \cdot 10^{-4}$	14	$1.07 \cdot 10^{-10}$	72	0.00
$5 \cdot 10^{-5}$	26	$7.31 \cdot 10^{-10}$	360	0.3
$2 \cdot 10^{-5}$	67	$1.51 \cdot 10^{-7}$	840	2.4

Table 9
Number of conjunctions and cumulative collision probability for different time spans of the reentry phase of a OneWeb (apogee/perigee: 1100 × 250) and a Starlink satellite (apogee/perigee: 550 × 300). For each column, we give the value for a low (first number) and a high solar activity second number).

Name	Time span (day)	$P_c^{cum,1sat}$	Conjunctions (<10 km)	Conjunctions (<1 km)
OneWeb	133/113	$2.33 \cdot 10^{-5}$/ $3.23 \cdot 10^{-7}$	6959/5040	12/4.3
Starlink	162/127	$7.17 \cdot 10^{-7}$/ $4.00 \cdot 10^{-12}$	1080/540	1.5/0.21

Declaration of Competing Interest

The authors declare that they have no known competing financial interests or personal relationships that could have appeared to influence the work reported in this paper.

Acknowledgements

The work of Alexis Petit was financed at 50% by POR FSE 2014–2020 in the framework of the Regione Toscana project Giovanis (www.giovanisi.it). The authors wish to thank the two anonymous referees whose useful comments helped to improve the paper.

References

Alessi, E.M., Rossi, A., Valsecchi, G., Anselmo, L., Pardini, C., Colombo, C., Lewis, H., Daquin, J., Deleflie, F., Vasile, M., et al., 2014. Effectiveness of gnss disposal strategies. Acta Astronaut. 99, 292–302.

Alessi, E.M., Schettino, G., Rossi, A., Valsecchi, G.B., 2018. Solar radiation pressure resonances in low earth orbits. Mon. Not. R. Astron. Soc. 473, 2407–2414.

Blake, R., Lewis, H., 2014. The effect of modelling assumptions on predictions of the space debris environment. In: Proceedings of the 65th International Astronautical Congress, Toronto.

Committee, I.A.S.D.C., et al., 2013. Stability of the future leo environment. IADC-12.08.

Flegel, S., Gelhaus, J., Wiedemann, C., Vorsmann, P., Oswald, M., Stabroth, S., Klinkrad, H., Krag, H., 2009. The master-2009 space debris environment model. In: Fifth European Conference on Space Debris.

Huang, S., Colombo, C., Alessi, E.M., Hou, Z., 2019. Large constellation de-orbiting with low-thrust propulsion. In: 29th AAS/AIAA Space Flight Mechanics Meeting, pp. 1–22.

Inter-Agency Space Debris Coordination Committee, 2007. IADC space debris mitigation guidelines. http://www. iadc-online.org/Documents/Docu/IADC_Mitigation_Guidelines_Rev1_Sep07.pdf.

Simon, J.L. et al., 1994. Numerical expressions for precession formulae and mean elements for the moon and the planets. Astron. Astrophys. 282, 663–683.

Klinkrad, H., 2006. Space Debris: Models and Risk Analysis. Springer Science & Business Media.

Shampine, L.F., Gordon, M.K., 1975. Computer Solution of Ordinary Differential Equations: the Initial Value Problem. Freeman, San Francisco, W.H.

Le May, S., Gehly, S., Carter, B., Flegel, S., 2018. Space debris collision probability analysis for proposed global broadband constellations. Acta Astronaut. 151, 445–455.

Lewis, H., Maclay, T., Lindsay, M., 2019. Long-term environmental effects of deploying the oneweb satellite constellation. In: 70th International Astronautical Congress, Washington DC, USA.

Lewis, H., Radtke, J., Rossi, A., Beck, J., Oswald, M., Anderson, P., Bastida Virgili, B., Krag, H., 2017. Sensitivity of the space debris environment to large constellations and small satellites. J. Br. Interplanet. Soc. 70, 105–117.

Lewis, H., Radtke, J., Rossi, A., Beck, J., Oswald, M., Anderson, P., Bastida Virgili, B., Krag, H., 2017. Sensitivity of the space debris environment to large constellations and small satellites. J. Br. Interplanet. Soc. 70, 105–117.

Liou, J.C., 2006. Collision activities in the future orbital debris environment. Adv. Space Res. 38, 2102–2106.

Petit, A., Lemaitre, A., 2016. The impact of the atmospheric model and of the space weather data on the dynamics of clouds of space debris. Adv. Space Res. 57, 2245–2258.

Pollard, J.E., 1997. Simplified approach for assessment of low-thrust elliptical orbit transfers. In: 25th International Electric Propulsion Conference, Cleveland, OH, pp. 97–160.

Radtke, J., Kebschull, C., Stoll, E., 2017. Interactions of the space debris environment with mega constellations–using the example of the oneweb constellation. Acta Astronaut. 131, 55–68.

Rossi, A., Anselmo, L., Pardini, C., Jehn, R., Valsecchi, G.B., 2009. The New Space Debris Mitigation (SDM 4.0) long term evolution code. In: Fifth European Conference on Space Debris, p. 90.

Rossi, A., Petit, A., McKnight, D., 2020. Short-term space safety analysis of leo constellations and clusters. Acta Astronaut.

Schaus, V., Radtke, J., Stoll, E., Rossi, A., Colombo, C., Tonetti, S., Holbrough, I., et al., 2017. Results of reference long-term simulations focussing on passive means to reduce the impact of space debris. In: 7th European Conference on Space Debris, ESA/ESOC, ESA, pp. 1–10.

Virgili, B.B., Dolado, J., Lewis, H., Radtke, J., Krag, H., Revelin, B., Cazaux, C., Colombo, C., Crowther, R., Metz, M., 2016. Risk to space sustainability from large constellations of satellites. Acta Astronaut. 126, 154–162.